



Mechanically interlocked pyrene-based photocatalysts

Amine Garci¹, Jacob A. Weber¹, Ryan M. Young ^{1,2}, Masoud Kazem-Rostami ¹, Marco Ovalle¹, Yassine Beldjoudi¹, Ahmet Atilgan¹, Youn Jue Bae¹, Wenqi Liu¹, Leighton O. Jones¹, Charlotte L. Stern ¹, George C. Schatz ¹, Omar K. Farha¹, Michael R. Wasielewski ^{1,2} and J. Fraser Stoddart ^{1,3,4,5} □

Triplet excited-state organic chromophores present countless opportunities for applications in photocatalysis. Here we describe an approach to the engineering of the triplet excited states of aromatic chromophores, which involves incorporating pyrene into pyridinium-containing mechanically interlocked molecules (MIMs). The π -extended nature of the pyrenes enforces $[\pi\cdots\pi]$ stacking, affording an efficient synthesis of tetrachromophoric octacationic homo[2]catenanes. These MIMs generate triplet populations and efficient intersystem crossing on account of the formation of a mixed charge-transfer/exciplex electronic state and a nanoconfinement effect, which leads to a high level of protection of the triplet state and extends the triplet lifetimes and yields. These compounds display excellent catalytic activity in photo-oxidation, as demonstrated by the aerobic oxidation of a sulfur-mustard simulant. This research highlights the benefits of using the mechanical bond to fine-tune the triplet photophysics of existing aromatic chromophores, providing an avenue for the development of unexplored MIM-based photosensitizers and photocatalysts.

yrene is a prototypical polycyclic aromatic hydrocarbon (PAH). It has been the subject 1-4 of extensive investigations in fundamental and applied photochemical research as an organic chromophore on account of its photophysical properties in solution and in the solid state. The functionalization of pyrene not only permits⁵⁻⁹ the fine-tuning of its optoelectronic properties at the molecular level, but also allows¹⁰⁻¹² control of the arrangement of molecules in the solid state to obtain a desired electronic performance. Compounds containing pyrene moieties and that maintain their monomeric integrity in the condensed state are well known to exhibit high fluorescence quantum yields 10,13 and long-lived excited states, features that are desirable in the development of organic light-emitting devices (OLEDs). The propensity of unhindered pyrene-based fluorophores¹⁴ to interact through $[\pi \cdots \pi]$ interactions at high concentrations and in the solid state often leads to quenching of the monomeric emission and the emergence of new emissions at lower energies associated with exciton delocalization between two or more molecules. The excimer/exciplex fluorescence of pyrene has been employed widely in sensors and probes for detecting environmental changes¹⁵⁻¹⁷, in guest molecules¹⁸⁻²⁰, in probing the structural properties of macromolecular systems^{21,22} and for the construction of photo-emissive organic materials, such as blue-light emitters, which are desirable for OLEDs^{23,24}. It has also been reported²⁵ that pyrene can be used as a photosensitizer for the generation of singlet oxygen (1O2) with high quantum yields in aqueous micellar solutions. More recently, a pyrene-based metal-organic framework has been utilized^{2,26-28} as a ¹O₂ photosensitizer for the heterogeneous photocatalysis of a sulfur-mustard simulant (half-life of $t_{1/2}$ = 5 min using 1 mol% catalyst). Notably, the most common strategy^{29–33} to enhance the singlet-triplet (S-T)

transformation is to use heavy atoms, because spin-orbit (λ) coupling becomes larger with increasing atomic number (Z). Other strategies such as intramolecular charge transfer (CT) in donor-acceptor (D-A) dyads have been employed³⁴ in the design of heavy-atom-free photosensitizers. For example, it has been reported34 that CT states formed in the boron-dipyrromethene-pyrene (BODIPY-pyrene, D-A) dyad as a result of photoinduced electron transfer recombine to yield the BODIPY triplet excited state. In the presence of molecular oxygen, BODIPY-pyrene dyads sensitize 1O2 with quantum yields of up to 0.75. More recently, efficient intersystem crossing (ISC) was achieved³⁵ by combining the spin-orbit coupling associated with heavy Br atoms in 1,3,5,8-tetrabromopyrene (TBP) and photoinduced electron transfer in a TBP⊂ExBox⁴⁺ host-guest complex supramolecular dyad. The efficient S-T transformation and ISC relaxation mechanisms play a central role in the enhancement of ¹O₂ generation and the subsequent increase in photocatalytic performance. Nevertheless, the formation of non-equilibrium host-guest complexes remains challenging and therefore the engineering of supramolecular systems displaying a persistent chemical superstructure and efficient S-T transformation is highly desirable in the pursuit of the development of organic photosensitizers and photocatalysts.

For more than half a century, mechanically interlocked molecules (MIMs) have attracted ^{36,37} interest based on their aesthetic appeal and for their applications in molecular switches and machines. Recently, considerable efforts have been devoted ^{38–50} to exploring the rich photochemical and materials properties of these exotic compounds. To achieve this goal, numerous luminophores have been utilized ^{38–50} to assemble MIMs for energy and electron transfer investigations. The mechanical bond presents the opportunity to control ^{51–54} the

Department of Chemistry, Northwestern University, Evanston, IL, USA. ²Institute for Sustainability and Energy at Northwestern, Northwestern University, Evanston, IL, USA. ³School of Chemistry, University of New South Wales, Sydney, New South Wales, Australia. ⁴Stoddart Institute of Molecular Science, Department of Chemistry, Zhejiang University, Hangzhou, China. ⁵ZJU-Hangzhou Global Scientific and Technological Innovation Center, Hangzhou, China. ⁵Ze-mail: stoddart@northwestern.edu

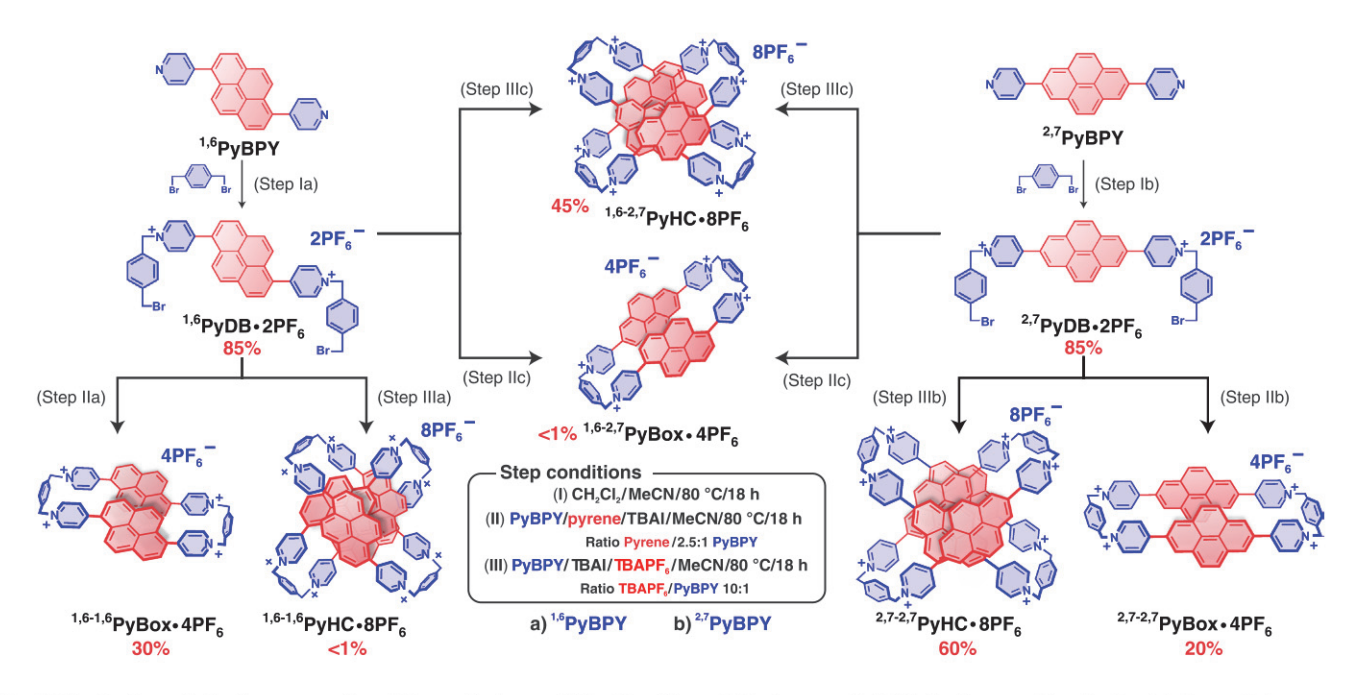


Fig. 1| Synthetic route for the preparation of the cyclophanes PyBox⁴⁺ and homo[2]catenanes PyHC⁸⁺. Syntheses of the dicationic intermediates ^{1,6}PyDB²⁺ (step Ia) and ^{2,7}PyDB²⁺ (step Ib). Syntheses of the cyclophanes ^{1,6-1,6}PyBox⁴⁺ (step IIa), ^{2,7-2,7}PyBox⁴⁺ (step IIb) and the cyclophane ^{1,6-2,7}PyBox⁴⁺ (step IIc). Syntheses of the octacationic homo[2]catenanes ^{1,6-1,6}PyHC⁸⁺ (step IIIa), ^{2,7-2,7}PyHC⁸⁺ (step IIIb) and ^{1,6-2,7}PyHC⁸⁺ (step IIIc).

arrangements of each component within a MIM, for example, in rigid and robust compounds such as rotaxanes and catenanes. This level of structural control lends itself to creating an excellent platform to fine-tune the optoelectronic properties of MIMs through careful selection of each molecular component. For example, refs. 39,41 describe a series of PAH-based rotaxanes (for example, pyrene or perylene) showing circularly polarized luminescence in solution, and refs. 42,44 report a white-light-emitting polymer that exhibits reversible on/off photoluminescence switching upon stretching and relaxation. In particular, pyridinium-based cyclophanes, such as cyclobis(paraquat-p-phenylene) (CBPQT⁴⁺) and its extended version (Ex"Box4+) have attracted attention on account of their ability to bind a wide range of PAHs in their cavities, affording asymmetrical D-A catenanes. These pyridinium-based MIMs are associated with valuable photophysical processes related to their applications in live-cell imaging⁴⁷, photodynamic therapy⁴⁶, energy storage⁵⁴ and photoinduced electron transfer reactions⁵⁵. The electrostatic interactions between the electron-deficient pyridinium-based cyclophanes and electron-rich PAH molecules not only drive the formation⁵⁶⁻⁵⁸ of inclusion complexes and/or MIMs, but also fine-tune the energy landscape of the D-A systems by promoting ultrafast intermolecular CT and triplet energy harvesting. Recently, we reported⁴⁷ the incorporation of an electron-rich anthracene moiety between two pyridinium units, which led to favourable $[\pi \cdots \pi]$ interactions, thereby promoting homo[2]catenane self-templation. This anthracene-based MIM exhibits low-energy fluorescence in the red optical region on account of the formation of a permanent exciplex system that can be detected in micromolar concentrations in cancerous living cells.

In this Article we report the one-pot synthesis of two constitutionally isomeric octacationic pyrene-based homo[2]catenanes, namely $^{2,7-2,7}\text{PyHC}^{8+}$ and $^{1,6-2,7}\text{PyHC}^{8+}$, in yields of 60% and 45%, respectively. The placement of pyrene between two pyridinium units linked by phenylene bridges not only allows the self-templated synthesis of these two homo[2]catenanes, as a result of the strong $[\pi\cdots\pi]$ interactions between the pyrene moieties and D–A CT interactions between pyridinium units and pyrene moieties, but also makes it possible to fine-tune the electronic properties of these compounds.

Steady-state absorption, fluorescence and transient absorption (TA) spectroscopies and density functional theory (DFT) calculations have revealed the dynamics associated with the mechanical bonds in the catenanes and their resulting photosensitization properties. The homogeneous photocatalytic activities of the homo[2] catenanes in the detoxification of the sulfur-mustard simulant, 2-chloroethyl ethyl sulfide (CEES), have been examined and compared to that of the free cyclophanes to highlight the role of exciplex fluorophores in enhancing the generation of singlet oxygen (${}^{1}O_{2}$).

Results

Synthesis and characterization. We used 1,6-bis-4-pyridyl-pyrene (1,6PvBPY) and 2,7-bis-4-pyridyl-pyrene (2,7PvBPY) as starting materials in the preparation (Fig. 1) of the two tetracationic cyclophanes ^{2,7-2,7}PyBox⁴⁺ and ^{1,6-1,6}PyBox⁴⁺, as well as the three octacationic homo[2]catenanes ^{2,7-2,7}PyHC⁸⁺, ^{1,6-1,6}PyHC⁸⁺ and ^{1,6-2,7}PyHC⁸⁺. Reaction (Fig. 1 and Supplementary Figs. 1 and 2) of the 1,6PyBPY or the ^{2,7}PyBPY with an excess of 1,4-dibromomethylbenzene led to isolation of the pure dicationic derivatives 1,6PyDB-2PF6 or ^{2,7}PyDB·2PF₆, respectively, in 85% yield. The formation of the octacationic homo[2]catenane ^{2,7-2,7}PyHC·8PF₆ (Fig. 1 and Supplementary Fig. 3) was performed by reacting ^{2,7}PyDB·2PF₆ with ^{2,7}PyBPY in the presence of a catalytic amount of tetrabutylammonium iodide (~20 mol%) and an excess of tetrabutylammonium hexafluorophosphate. This self-templated synthesis exclusively produced, in a single step, the homo[2]catenane ^{2,7-2,7}PyHC·8PF₆ in 60% yield. The free cyclophane ^{2,7-2,7}PyBox·4PF₆ was obtained in 20% yield by reacting (Fig. 1 and Supplementary Fig. 4) the same aforementioned precursors, employing pyrene as a template. Following a similar synthetic route to that used in the preparation of ^{2,7-2,7}PyHC·8PF₆, reacting ^{1,6}PyBPY with ^{1,6}PyDB·2PF₆ produced (Fig. 1 and Supplementary Fig. 5) the cyclophane 1,6-1,6PyBox-4PF₆ as a major product in 30% yield and the catenane 1,6-1,6PyHC-8PF,6 in 1% yield (Fig. 1 and Supplementary Fig. 6). Starting with a combination of either ^{2,7}PyDB·2PF₆ with ^{1,6}PyBPY or ^{1,6}PyDB·2PF₆ with ^{2,7}PyBPY afforded (Fig. 1 and Supplementary Fig. 7) the asymmetric homo[2]catenane 1,6-2,7PyHC-8PF6 in good yields (45%) in both cases.

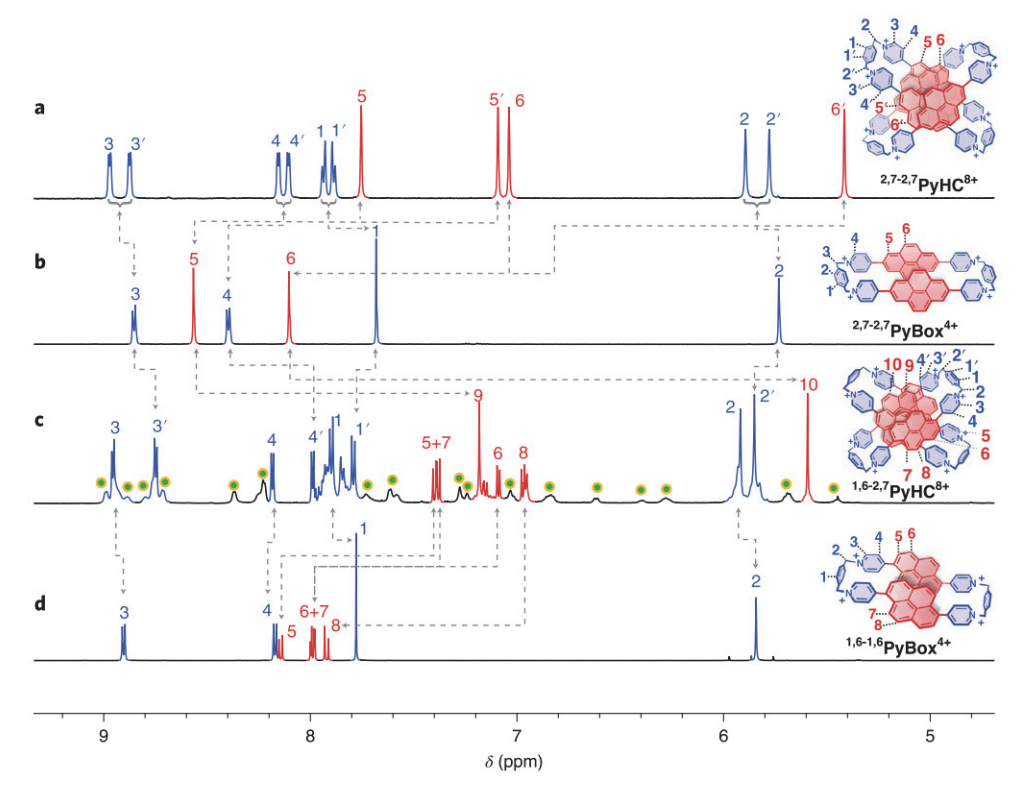


Fig. 2 | 'H NMR spectra of the cyclophanes and homo[2]catenanes. a, 'H NMR spectrum of ^{2,72,7}PyHC⁸⁺. b, 'H NMR spectrum of ^{2,7-2,7}PyBox⁴⁺. c, 'H NMR spectrum of ^{1,6-2,7}PyHC⁸⁺. d, 'H NMR spectrum of the ^{1,6-1,6}PyBox⁴⁺.

To study the self-templation process, the K_a value of the 2,7 PyB $^{2+}$ C $^{2,7-2,7}$ PyB $^{2+}$ complex, as calculated (Supplementary Figs. 8 and 9) from 1 H NMR titration experiments, was found to be $(4.38\pm0.64)\times10^{3}$ M $^{-1}$, that is, almost 56 times larger than the K_a value of the 1,6 PyB $^{2+}$ C $^{1,6-1,6}$ PyB $^{2+}$ complex (78.1 ± 1.3) M $^{-1}$, indicating that the strong $[\pi\cdots\pi]$ interactions between the 2,7 PyD $^{2+}$ units are the main driving force for the efficient synthesis of the $^{2,7-2,7}$ PyHC 2,7 PyH $^$

The ¹H NMR spectrum of the symmetrical ^{2,7-2,7}PyHC⁸⁺ homo[2] catenane shows (Fig. 2) the presence of 12 resonances, that is, double the number compared to those present in the ¹H NMR spectrum resulting from the corresponding cyclophane, 2,7-2,7PyBox4+. This doubling of resonances for the catenane is expected, because the union of two cyclophanes generates internal and external regions, both of which result in hydrogens that reside in these non-equivalent chemical environments. As a result, distinct ¹H NMR signals arise from the two ^{2,7}PyDB²⁺ units on each equivalent ring, which can either reside in the enclosed or peripheral chemical environments. The resonances for the inside pyridinium protons (H₃, H₄) of ^{2,7-2,7}PyHC⁸⁺ are slightly shifted (δ =8.87 and 8.10 ppm) relative to the comparable protons ($\delta = 8.85$ and 8.40 ppm) for $^{2,7-2,7}$ PyBox⁴⁺. The most upfield resonance of ^{2,7-2,7}PyHC⁸⁺ arises from the internal pyrene protons, H_{6} , which resonate at 5.41 ppm, when compared with the equivalent proton in the ^{2,7-2,7}**PyBox**^{$\bar{4}+$}, which resonate at δ =8.10 ppm. This shielding effect in the pyrene-based catenane arises from strong pyrene $[\pi \cdots \pi]$ stacking and intramolecular CT interactions.

The homo[2]catenane ^{1,6-2,7}**PyHC**·8PF₆, has lower symmetry and therefore displays (Fig. 2) a much more complicated ¹H NMR spectrum than that obtained for ^{2,7-2,7}**PyHC**·8PF₆. The ¹H signals of ^{1,6-2,7}**PyHC**⁸⁺, which are most diagnostic of the formation of a homo[2] catenane, are the proton resonances of the pyrene moieties of the ^{2,7}PyDB²⁺ and ^{1,6}PyDB²⁺ units, which become strongly shielded in the catenane, resulting in the observed upfield chemical shift of these resonances relative to those of the free cyclophane. For example,

the resonances for the pyrene protons in the 1,6PyDB²⁺ units within $^{1,6-2,7}$ PyHC⁸⁺ are shifted slightly upfield (δ =7.40-6.97 ppm), compared with those near $\delta = 8.14-7.98 \,\mathrm{ppm}$ for the comparable cyclophane, 1,6-1,6PyBox4+. This observation is in stark contrast to the two resonances corresponding to the eight hydrogens of the ^{2,7}PyDB²⁺ units, which are shifted substantially upfield to (δ =7.18 and 5.60 ppm) when incorporated into 1,6-2,7PyHC8+. These shielding effects are evidence that the ^{2,7}PyDB²⁺ units are positioned inside the catenane, whereas the 1,6PyDB2+ units reside outside. This selectivity is expected because the $[\pi \cdots \pi]$ stacking is stronger in the 2,7-constitution, which is less twisted and distorted than the 1,6-constitution. Another broad set of signals were observed at room temperature, an observation that can be attributed to the asymmetric nature of the 1,6-2,7PyHC8+ component ring(s) and the more rigid and compact structure of the catenane. A detailed investigation of the dynamic behaviour and different co-conformations—resulting from relative motion between the mechanically interlocked rings of the catenanes using line-shape analysis—is described in Supplementary Note 1 and Supplementary Figs. 10–14.

The solid-state (super)structures of cyclophanes ^{1,6-1,6}**PyBox**⁴⁺ (Fig. 3a,c) and ^{2,7-2,7}**PyBox**⁴⁺ (Fig. 3b,d) were obtained from single-crystal X-ray crystallography. The ^{2,7-2,7}**PyBox**⁴⁺ shows a symmetrical box-like cyclophane with a cavity measuring 18.9 Å in length and 6.3 and 6.6 Å in width at its periphery and centre, respectively. Conversely, ^{1,6-1,6}**PyBox**⁴⁺ is characterized by a distorted box-like geometry as the result of the large torsional angles between the pyrene and the two pyridinium units at the 1- and 6-positions. The torsional angles of 54° and 51° between the pyrene and pyridinium units are much higher than observed (~25°) in the original ^{2,7-2,7}**PyBox**⁴⁺. The truncated cavity size created by the pyrene–pyridinium steric strain results in a low binding affinity of the ^{1,6}**PyDB**²⁺C^{1,6-1,6}**PyBox**⁴⁺ complex, and explains the lower yield (1%) obtained in the synthesis of ^{1,6-1,6}**PyHC**⁸⁺ compared to that (45%) of ^{2,7-2,7}**PyHC**⁸⁺.

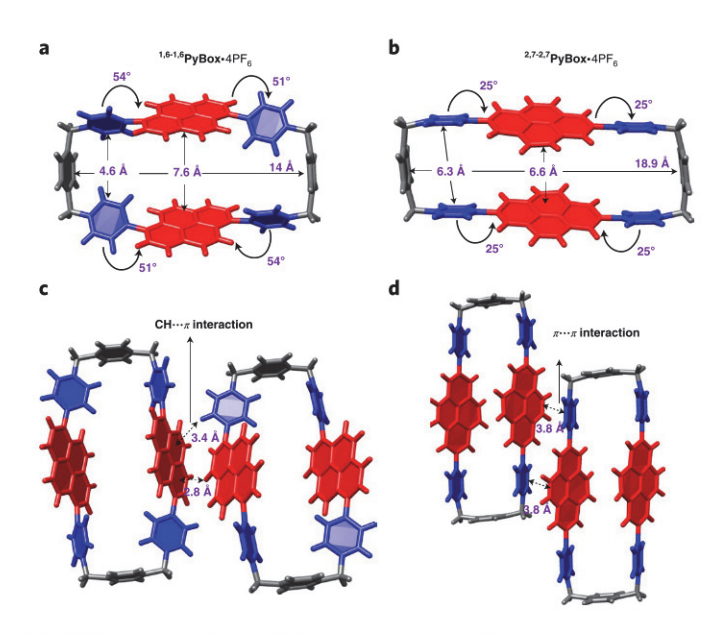


Fig. 3 | Crystal structures of the cyclophanes. a,c, Crystal structure of 1,6-1,6**PyBox**⁴⁺(**a**) and the packing of the solid-state structure displays intermolecular CH··· π interactions between the pyrenes (**c**). **b,d**, Crystal structure of $^{2,7-2,7}$ **PyBox**⁴⁺(**b**) and the packing of the solid-state structure displays intermolecular π ··· π interactions between the pyrenes (**d**). PF₆-counterions are omitted for the sake of clarity.

The solid-state (super)structure of catenane $^{2,7-2,7}$ PyHC·8PF $_6$ reveals (Fig. 4) that the mechanically interlocked pyrenes have interplanar $[\pi \cdots \pi]$ distances of 3.4 Å. The torsional angles (Fig. 4c) between the two mechanically interlocked cyclophanes are 119° and 61°. The pyrene moieties within the catenane structure are engaged in $[\pi \cdots \pi]$ stacking and D–A interactions with the pyridinium units. The one-dimensional (1D) stacking of the catenanes along the a axis (Fig. 4b) is governed by $[\pi \cdots \pi]$ interactions between pyrene moieties.

Steady-state optical characterizations. The effect of extending the conjugation length of pyrene by substitution at the 1,6- and 2,7-positions with pyridine units not only leads to different topological and structural features, but also to fine-tuning⁵⁹ of the electronic and luminescent properties of the pyrenes. Absorption and fluorescence studies were carried out in solution to unravel the effect of the mechanical bond on the photophysical properties of the pyrenes incorporated within the PyHC⁸⁺ homo[2]catenanes. The optical parameters are summarized in Table 1.

The absorption data for PyDB²⁺ reveals (Supplementary Figs. 15 and 16) a bathochromic shift compared⁵⁹ to the neutral PyBPY $\{(^{1.6}\text{PyBPY}, \lambda_{\text{max}} = 358 \text{ nm}; ^{1.6}\text{PyDB}^{2+}, \lambda_{\text{max}} = 420 \text{ nm}), (^{2.7}\text{PyBPY}, \lambda_{\text{max}} \approx 290 \text{ nm}, ^{2.7}\text{PyDB}^{2+}, \lambda_{\text{max}} = 322 \text{ nm})\}$ as a result of the augmented CT character in the dicationic systems. The macrocyclization step to form the cyclophanes does not lead to any notable changes in the absorption band of the PyBox4+. This observation was anticipated because of the large distance (~7 Å) between the two pyrenes, which causes these chromophores to behave as separate entities. Conversely, in the case of the homo[2]catenanes, the chromophores of the two cyclophanes are positioned via the mechanical bond and noncovalent attractive forces to be in proximity to one another (~3.5 Å), leading (Fig. 5a) to a bathochromic broadening with loss of features but no changes in the λ_{max} of absorption when compared to that for the cyclophane. The shift of the absorption wavelengths caused by mechanical confinement is more pronounced in the case of the asymmetric catenane 1,6-2,7PyHC8+ for the two bands arising (Supplementary Fig. 17) from the 1,6-pyrene

chromophore and the 2,7-pyrene chromophore. In the case of the 1,6-pyrene band there is a 20-nm bathochromic shift compared to that in $^{1,6-1,6} \mathbf{PyBox^{4+}}$. Additionally, the 2,7-pyrene band was broadened asymmetrically to a greater extent than was observed for the $^{2,7-2,7}\mathbf{PyHC^{8+}}$, along with a bathochromic shift of 15 nm in λ_{\max} . The greater effect of the mechanical bond on the absorption properties in the $^{1,6-2,7}\mathbf{PyHC^{8+}}$ is in agreement with the higher restricted confinement within this asymmetric homo[2] catenane compared with the situation in the symmetric analogue $^{2,7-2,7}\mathbf{PyHC^{8+}}$.

The evolution of the emissive properties ongoing from PyDB2+ to PyBox4+ to PyHC8+ has also been explored. The enhanced CT resulting from the cationic nature of PyDB²⁺ causes a redshifted emission (Supplementary Figs. 18 and 19) compared⁵⁹ to the uncharged PyBPY counterparts {(1.6PyBPY, $\lambda_{\text{max}} = 400 \text{ nm}; \frac{1.6}{\text{PyDB}^2+}, \lambda_{\text{max}} = 537 \text{ nm}), (2.7PyBPY, \lambda_{\text{max}} \approx 420 \text{ nm}, \frac{2.7}{\text{PyDB}^2+}, \frac{2.7}{\text{PyD$ λ_{max} = 551 nm)}. The macrocyclization has a marked effect on the fluorescence spectrum of 1,6-1,6PyBox4+, with a bathochromic shift of 25 nm compared to the corresponding dicationic precursor 1,6PyDB2+: however, there was no change in the emission of the ^{2,7-2,7}PyBox⁴⁺ analogue. The photoluminescence spectra of the homo[2]catenanes PyHC8+ show (Fig. 5b) pronounced differences compared to those obtained for the cyclophanes PyBox4+. ^{2,7-2,7}PyBox⁴⁺ has a single emission peak at 554 nm, whereas ^{2,7-2,7}PyHC⁸⁺ has a broad featureless exciplex peak centred on 593 nm. The bathochromic shift in the emission wavelength in 1,6-2,7PyHC8+ $(\lambda_{\text{max}} = 603 \text{ nm})$ was greatest when compared to either of the fluorescence spectra observed for the cyclophanes and ^{2,7-2,7}PyHC⁸⁺. Again, this enhanced exciplex character compared to the 2,7 system is a result of the close proximity of the chromophores in the 1,6-2,7PvHC8+. The exciplex emission of 1,6-2,7PvHC8+ is produced when we excite either the 1,6- or the 2,7-pyrene and is a result of intramolecular interactions between the two regioisomers, as confirmed by the excitation spectrum (Supplementary Fig. 20). The steadystate results highlight the formation of exciplexes upon irradiation of the pyrene-based homo[2]catenanes. The enhancement of this effect occurs on account of greater constrictive nanoconfinement by the pyrene units within the tighter catenane, 1,6-2,7 PyHC8+.

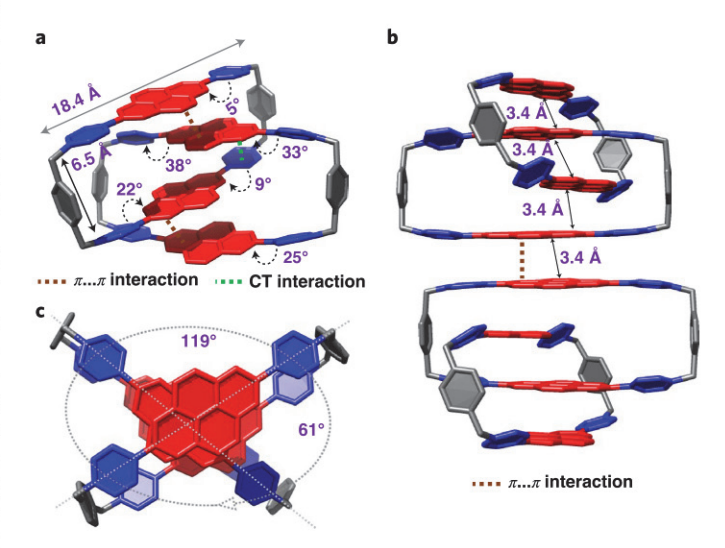


Fig. 4 | Solid-state (super)structure of the homo[2]catenane $^{2,7-2,7}$ **PyHC**⁸⁺. **a**, Plan view of the crystal structure of $^{2,7-2,7}$ **PyHC**⁸⁺, showing the geometry of the molecule. **b**, The packing of the solid-state structure of $^{2,7-2,7}$ **PyHC**⁸⁺ displays intermolecular $[\pi\cdots\pi]$ interactions between the pyrene units. **c**, Side-on view of the crystal structure of $^{2,7-2,7}$ **PyHC**⁸⁺, showing the dihedral angles between the two mechanically interlocked cyclophanes. PF₆⁻ counterions are omitted for the sake of clarity.

| Table 1 Spectroscopic parameters of the PyDB ²⁺ derivatives, ^{1,6-1,6} PyBox ⁴⁺ , ^{2,7-2,7} PyBox ⁴⁺ cyclophanes and ^{2,7-2,7} PyHC ⁸⁺ , ^{1,6-2,7} PyHC ⁸⁺ homo[2]catenanes | | | | | | | |
|--|----------------------|----------------------------|---------------|---------------------|------------------|---------------------|-------|
| Compounda | λ_{abs} (nm) | λ_{em} (nm) | τ_1 (ps) | τ ₂ (ps) | $\tau_{_3}$ (ns) | τ ₄ (ns) | Φ (%) |
| ^{1,6} PyDB ²⁺ | 422 | 537 | - | - | | - | 49 |
| ^{2,7} PyDB ²⁺ | 322 | 551 | 0.7 ± 0.3 | 180 ± 10 | 14.7 ± 0.6 | 265±8 | 22 |
| ^{1,6-1,6} PyBox ⁴⁺ | 421 | 562 | 0.7 ± 0.3 | 310 ± 8 | 8.6 ± 0.6 | 905±40 | 40 |
| ^{2,7-2,7} PvBox ⁴⁺ | 320 | 554 | 1.3 + 0.3 | 260+8 | 14.9 + 0.7 | 320+10 | 11 |

 λ_{absr} absorption wavelength; λ_{emr} emission wavelength; τ_{tr} time constant of the CT/exciplex formation; τ_{2r} time constant of the relaxation; τ_{1r} , time constant of the CT/exciplex lifetime; τ_{1r} , time constant of the triplet lifetime; σ (%), fluorescence quantum yield.

 69 ± 3

 22 ± 2

 15.8 ± 0.6

 22.4 ± 0.6

 760 ± 40

 $2,800 \pm 200$

9

~0.3

 0.7 ± 0.3

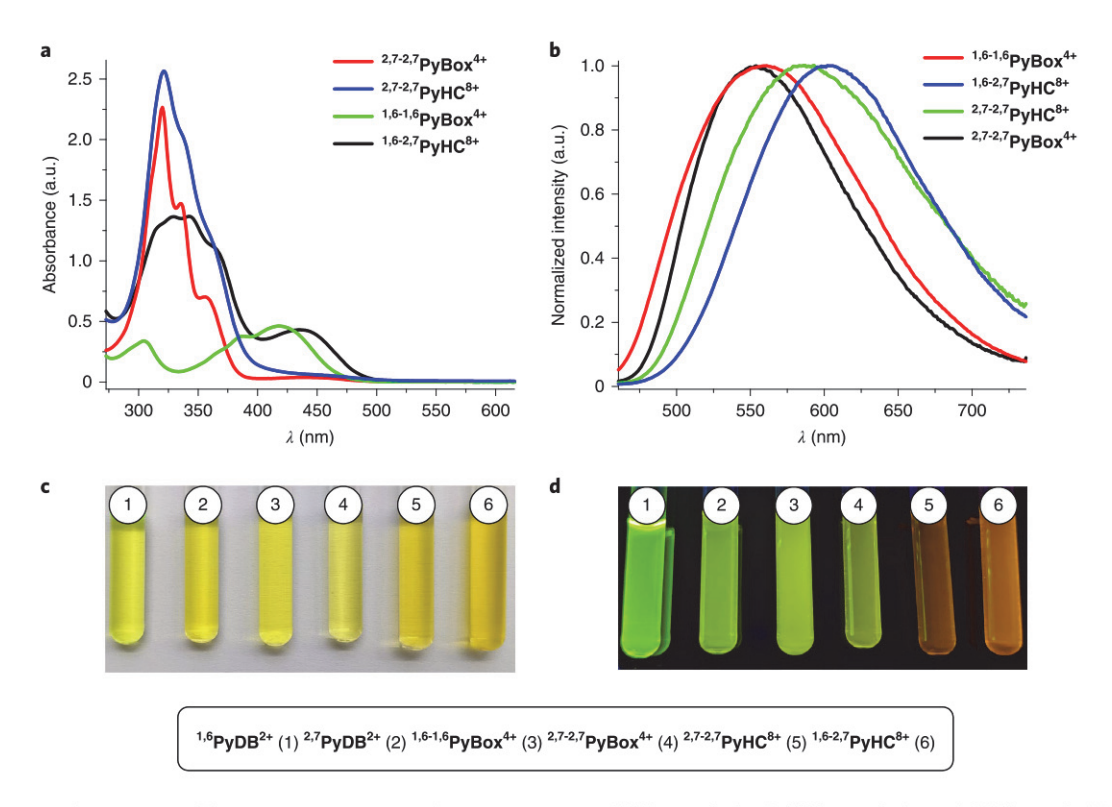


Fig. 5 | Steady-state absorption and fluorescence spectra. a, Absorption spectra of $^{2,7-2,7}$ PyBox⁴⁺ (red), $^{1,6-1,6}$ PyBox⁴⁺ (green), $^{2,7-2,7}$ PyHC⁸⁺ (blue) and $^{2,7-1,6}$ PyHC⁸⁺ (black) in MeCN. **b**, Fluorescence spectra of $^{2,7-2,7}$ PyBox⁴⁺ (black), $^{1,6-1,6}$ PyBox⁴⁺ (red), $^{2,7-2,7}$ PyHC⁸⁺ (green) and $^{2,7-1,6}$ PyHC⁸⁺ (blue) in MeCN. **c**, Photograph of the different solutions of cyclophanes and catenanes in MeCN upon irradiation with a UV lamp ($λ_{exc}$ = 364 nm).

Transient absorption studies. We performed TA spectroscopy to determine the nature of the excited-state dynamics in the pyrene-based cyclophanes and homo[2] catenanes in deaerated solution at room temperature. Beginning with the dicationic derivative ^{2,7}**PyDB**²⁺, upon excitation at 330 nm (Supplementary Figs. 21 and 22), features at 440 and 540 nm convert rapidly within ~700 fs to a spectrum with peaks at 415 and 510 nm. We assign this conversion to the rapid formation of a CT-like state resulting from D–A interactions between the pyrene and pyridinium units, which is corroborated by the CT-like emission that is common between ^{2,7}**PyDB**²⁺, the cyclophanes and catenanes. This state then relaxes in 180 ps and forms a triplet in 15 ns that survives for ~265 ns before undergoing diffusional quenching.

Similar spectra are observed (Supplementary Figs. 23—26) in ^{2,7-2,7}**PyBox**⁴⁺ and ^{2,7-2,7}**PyHC**⁸⁺. Each forms the CT state within ~1 ps and creates a triplet with a 15- and 16-ns time constant, respectively.

The excited-state dynamics in 2,7-2,7PyHC8+ are not dramatically different from those of 2,7-2,7PyBox4+ or 2,7PyDB2+, with the principal difference being the rate of appearance of the CT state. The spectral features of the CT state in 2,7-2,7PyHC8+ are broader than those of the cyclophane because of the $\pi \cdot \cdot \cdot \pi$ interactions between the interacting pyrene moieties. The CT relaxation time is different between each free cyclophane and the homo[2]catenane, occurring in 260 ± 8 ps in the case of $^{2,7-2,7}$ PyBox⁴⁺ and 69 ± 3 ps in the case of ^{2,7-2,7}PyHC⁸⁺ as the geometry of the cyclophane and the solvent relax to accommodate the new charge distribution. Stronger interactions between the π surfaces in ^{2,7-2,7}**PyHC**⁸⁺ most probably inhibit complete relaxation, resulting in a shallower potential energy trap and hence a shorter lifetime for the unrelaxed CT state. A longer triplet lifetime is also observed in ^{2,7-2,7}PyHC⁸⁺ compared to that in $^{2,7-2,7}$ PyBox⁴⁺ (760 ± 40 ns versus 320 ± 10 ns). The large redshift in the steady-state fluorescence (Fig. 5b) of ^{2,7-2,7}PyHC⁸⁺ suggests that

^{2,7-2,7}PyHC⁸⁺

1,6-2,7PvHC8+

321

343-436

593

603

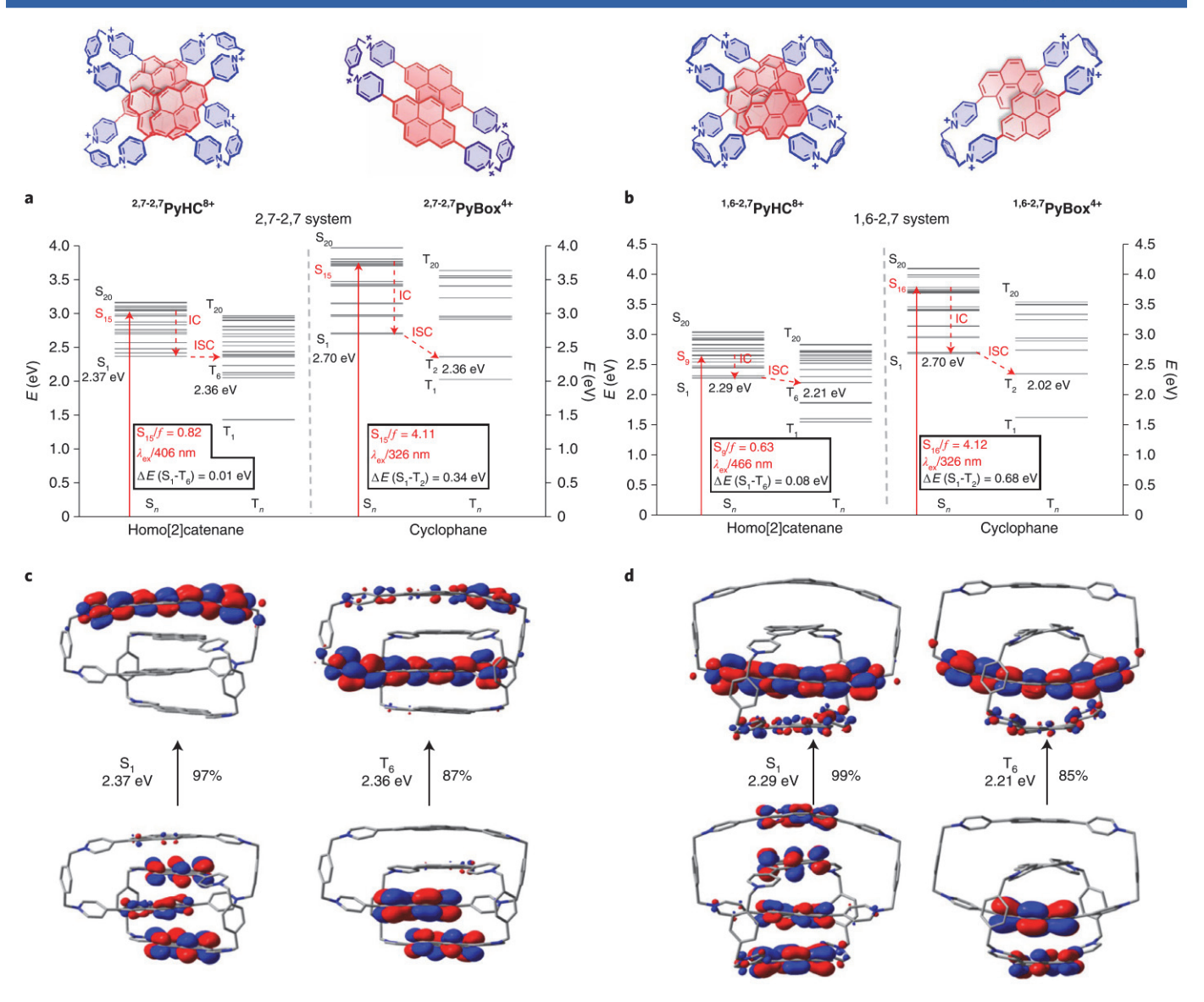


Fig. 6 | Calculated energy-level diagrams of the singlet (S_n) and triplet (T_n) transitions. a, Energy-level diagrams for cyclophane $^{2,7-2,7}$ PyBox⁴⁺ and the homo[2]catenane $^{2,7-2,7}$ PyHC⁸⁺. **b**, Energy-level diagrams for cyclophane $^{1,6-2,7}$ PyBox⁴⁺ and the homo[2]catenane $^{1,6-2,7}$ PyHC⁸⁺. **c**, NTOs (hole NTOs on top and electron NTOs on bottom) for the S₁ and T₆ transitions of $^{2,7-2,7}$ PyHC⁸⁺. **d**, NTOs for the S₁ and T₆ transitions of $^{1,6-2,7}$ PyHC⁸⁺. **f**, Oscillator strength.

the emissive state may be an exciplex, which is possible given the short distance between the pyrene units in the homo[2]catenane. The slightly longer lifetime compared to ^{2,7-2,7}PyBox⁴⁺ may be a result of such a state: the similarity in the spectra between ^{2,7-2,7}PyHC⁸⁺ and ^{2,7-2,7}PyBox⁴⁺, however, suggests that the coupling between the pyrene units is relatively weak.

The different constitutions of the pyrenes lead to some changes in the excited-state spectra and kinetics. Supplementary Figs. 27 and 28 show the TA spectra for ^{1,6-1,6}**PyBox**⁴⁺ excited at 414 nm. The initial locally excited state exhibits a maximum at 562 nm, along with a ground-state bleach at 420 nm and a brief stimulated emission band at ~480 nm. These features decay in 0.8 ps to a broadened excimer-like spectrum with peaks at 490 and 555 nm that evolve over the next ~300 ps into a relaxed excimer where the 480-nm feature dominates. Triplet formation occurs in 8.6 ns, that is, faster than in ^{2,7}**PyDB**²⁺ and ^{2,7-2,7}**PyBox**⁴⁺, which is most likely a result of the lower energy.

The TA data for ^{1,6-,2,7}**PyHC**⁸⁺ excited at 414 nm and accompanying global analysis are shown in Supplementary Figs. 29 and 30. The transient spectra exhibit a ground-state bleach at 350 nm, which

is intermediate between the 1,6- and 2,7-constituted cyclophanes, and a minimum at 458 nm. The locally excited state undergoes a similar 0.7-ps deactivation to form a CT-like state. No difference was observed when the sample was excited at 330 nm, suggesting that ultrafast energy transfer between the higher-energy pyrene is occurring within the ~300-fs instrument resolution when excited with ultraviolet (UV) light. The CT state relaxes in 22 ps, which is again faster than that of the cyclophanes, and may suggest hindered nuclear motion on account of the strong [π ··· π] interactions of the pyrenes. The spectra (Supplementary Figs. 29 and 30) of these unrelaxed and relaxed CT states are similar to that of the CT state of 1,6-1,6**PyBox**⁴⁺, although the peak at 416 nm more strongly resembles the CT state spectra of the 2,7-constituted compounds. The relaxed excimer state then converts to the triplet state in 22 ns before diffusional quenching in ~2 µs.

The longer CT-like state lifetime (22 ns) and the redshifted emission in ^{1,6-2,7}PyHC⁸⁺ may suggest the formation of an exciplex between the interacting electronically distinct pyrenes in the catenane, with an increased CT character of the excited state that decreases the ability to couple to the electric field and lowers the

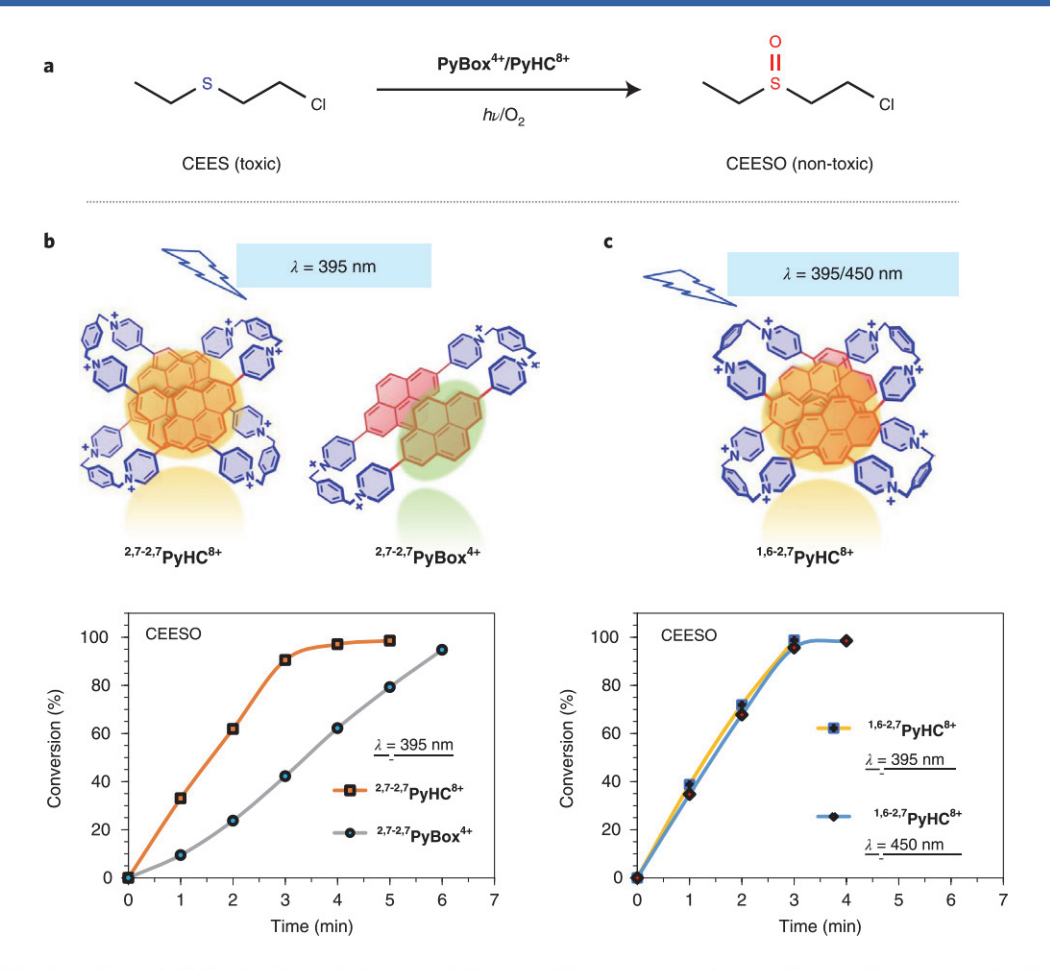


Fig. 7 | Photosensitized catalysis of CEES using the cyclophanes and the homo[2]catenanes as photocatalysts. a, Reaction equation for the photocatalytic aerobic oxidation (detoxification) of the sulfur-mustard simulant (CEES) using the cyclophanes and the homo[2]catenanes as photocatalysts. **b**, Homogeneous photocatalysis of CEES in CD₃OD using homo[2]catenane ^{2,7-2,7}**PyHC**⁸⁺ (0.5 mol%) and cyclophanes ^{2,7-2,7}**PyBox**⁴⁺ (1mol%). **c**, Homogeneous photocatalysis of CEES in CD₃OD using the homo[2]catenane ^{1,6-2,7}**PyHC**⁸⁺ (0.5 mol%). The conversion curves have been obtained from the appearance of CEESO.

emission yield. The spectrum of this exciplex shares features common to both the 1,6- and 2,7-substituted pyrene CT states, supporting the involvement of both constitutions within this state. Exciplex formation is favoured in ^{1,6-2,7}PyHC⁸⁺ on account of the electronically distinct nature of the neighbouring pyrenes within the catenane structure, with the orbital overlap between the differently functionalized pyrenes leading to stronger inter-pyrene CT coupling compared to the ^{2,7-2,7}PyHC⁸⁺ system.

Importantly, 1,6-2,7PyHC8+ generates the highest amount of triplet of the compounds studied based on the relative absorption of the long-lived signal to that of the emitting species, despite having the longest CT-like state lifetime. Efficient triplet generation would typically be expected to be accompanied by a rapid deactivation process; in this case, however, the longer lifetime of the exciplex species enables mixing of the spins between the partially charge-separated entities and the acquisition of triplet character to the wavefunction. The availability of triplet energy levels and the energy gap between the CT/exciplex and triplet states has been explored computationally. From the relative intensities in the TA data (Supplementary Figs. 23—26), the triplet yield of ^{2,7-2-7}PyHC⁸⁺ appears to be lower than that of the ^{2,7-2,7}PyBox⁴⁺ cyclophane, although both generate substantial triplet populations. The mechanically interlocked structure may also afford some level of protection of the triplet to diffusional quenching, a property that may extend the triplet lifetime. The higher triplet yield in 1,6-2,7PyHC8+ correlates well with the photocatalytic performance.

Computational studies. To gain deeper insight into the photophysical characteristics of the pyrene-based cyclophanes and homo[2] catenanes, quantum chemical DFT calculations were performed to explore the singlet and triplet excited states. The natural transition orbitals (NTOs) were calculated (Fig. 6 and Supplementary Figs. 31 and 32) for the S_1 and T_6 transitions of the pyrene-based homo[2] catenanes, and for the S_1 and T_2 transitions of the pyrene-based cyclophanes. These NTO calculations yielded condensed orbital representations of the electron and the hole residencies for each state that have the highest probability of participating in the ISC mechanism.

The line shapes and transition energies of the generated UV-vis spectra for the cyclophanes and homo[2]catenanes were in good agreement with the experimentally obtained UV-vis spectra (Supplementary Figs. 33–37). The energy-level diagrams for the first 20 singlet and triplet transitions are displayed in Fig. 6 for the 2,7-2,7 (Fig. 6a) and 1,6-2,7 (Fig. 6b) pyrene-based cyclophanes and homo[2]catenanes. The energy-level diagrams of the cyclophanes are presented in Supplementary Fig. 38, including ^{1,6-1,6}PyBox⁴⁺ for comparison. The effects that the mechanical bond imparts on the electronic characteristics of the pyrene-based chromophores become clear when the singlet and triplet transition energies of the cyclophanes are compared with those of the corresponding homo[2]catenanes. Furthermore, assessment of these transition energy diagrams indicates different excited-state behaviour in ^{2,7-2,7}PyHC⁸⁺ and ^{1,6-2,7}PyHC⁸⁺, which can be attributed in part to the

more restrictive nature of the nanoconfinement present within the 1,6-2,7 homo[2]catenane.

As expected based on the fluorescence spectra (Fig. 5b), the energies of the first excited-state singlets (S₁) of the homo[2]catenanes are lowered relative to those in the corresponding free cyclophanes. This observation is consistent with the experimental (Fig. 5b) bathochromic emission bands of 2,7-2,7PyHC8+ and 1,6-2,7PyHC8+ relative to those of their respective pyrene-based cyclophanes, $^{2,7-2,7}$ **PyBox**⁴⁺ and $^{1,6-2,7}$ **PyBox**⁴⁺. The T_n state energies of the pyrene homo[2]catenanes also decreased relative to those calculated for their corresponding free pyrene cyclophanes. The homo[2]catenane 1,6-2,7PyHC8+, with its tighter conformational constriction, is expected to be especially efficient at generating the triplet state with a $\Delta E S_1/T_1$ that is less than half that of the calculated $\Delta E S_1/T_1$ T₁ value for the more co-conformationally free homo[2]catenane, ^{2,7-2,7}PyHC⁸⁺. Moreover, ^{1,6-2,7}PyHC⁸⁺ has a substantial amount of overlap between the hole NTOs for the S₁ and T₆ transitions (Fig. 6d) compared to the minimal overlap that exists (Fig. 6c) between the hole NTOs for the same states of ^{2,7-2,7}PyHC⁸⁺. This difference in the hole-NTO overlaps provides evidence that the ISC efficiency of the 1,6-2,7PyHC8+ is greater than that of the 2,7-2,7PyHC8+.

Another observation that is consequential for the efficiency of ISC within the pyrene-based homo[2]catenanes is the density of triplet states, which is much higher compared to their pyrene-based cyclophane counterparts. This enhancement in the density of states is especially evident when the visualization of the transition energy-level diagrams is expanded to include 20 states for both the singlet and triplet manifolds (Fig. 6). A greater density of states increases the probability that a triplet state will have approximately the same energy as S_1 , which, according to Kasha's rule, is the most likely state to cross into the triplet manifold on account of the rapid non-radiative relaxation from upper electronic states. Indeed, T_6 and S_1 have small energy differences for both ${}^{2,7\text{-}2,7}\text{PyHC}^{8+}$ (ΔE $S_1/T_6 \approx 0.01\,\text{eV}$) and ${}^{1,6\text{-}2,7}\text{PyHC}^{8+}$ (ΔE $S_1/T_6 \approx 0.08\,\text{eV}$), indicating exceptionally efficient channels for the population of the triplet manifolds of the pyrene-based homo[2] catenanes.

The last noteworthy comparison to make between the pyrene-based cyclophanes and the corresponding homo[2]catenanes pertains to the CT nature of the S₁ state. In both cases, the $S_0 \leftrightarrow S_1$ transitions are CT transitions, as can be ascertained through the graphic depiction of excited-state electron migration in the electrostatic potential difference maps within Supplementary Figs. 39-41. For the two pyrene-based cyclophanes, the highest occupied NTO (HONTO) is localized to one pyrene unit, and the lowest unoccupied NTO (LUNTO) is distributed across ^{2,7}PyDB²⁺ with a high residency on the pyridinium rings. The CT nature of the S₁ transitions of pyrene-based homo[2]catenanes is very different from that of the free cyclophanes. The S₁ HONTOs of both ^{2,7-2,7}PyHC⁸⁺ and ^{1,6-2,7}PyHC⁸⁺ are localized on one external pyrene chromophore, and the LUNTO resides on the nearest pyrene, that is, on the opposite cyclophane and located inside the catenane. This disparity between the residency of the HONTO and LUNTO affords S₁ CT transitions that are completely disjointed (negligible overlap between HONTO/LUNTO) and, as a consequence, oscillator strengths that approach zero. The highly disjointed CT nature of the excited states of ^{2,7-2,7}PyHC⁸⁺ and ^{1,6-2,7}PyHC⁸⁺ is consistent with their correspondingly low quantum yields of fluorescence (9.4 and 8.3%, respectively).

Based on the time-dependent (TD)-DFT data, we have devised a general mechanism for enhancing the efficiency of populating the triplet states through the formation of the mechanical bond. Absorption of a photon excites the homo[2] catenane into an upper singlet excited state (S_n) that then relaxes quickly to S_1 through internal conversion (IC). Subsequent to populating S_1 , ISC takes place to an upper triplet state. This mechanism is made more efficient by the nanoconfinement of the pyrene chromophores within

 $^{2,7-2,7}$ PyHC⁸⁺ and $^{1,6-2,7}$ PyHC⁸⁺ that increases the density of the triplet states and therefore the probability of a triplet state being of comparable energy as the principal singlet excited state (S_1).

Photocatalysis studies. On account of the promising ISC and triplet population capabilities induced by the mechanical bonds within the pyrene-based homo[2]catenanes, we decided to use this platform to explore the differences in photocatalytic behaviour of our cyclophanes and catenanes and investigate the differing extent of mechanical-bond-induced constraint between the looser 2,7-2,7 and the tighter 1,6-2,7 homo[2]catenanes. To this end, we investigated the homogeneous photocatalytic activities of both the cyclophanes and homo[2]catenanes in the detoxification of the sulfur-mustard simulant, CEES.

Photocatalysis of CEES with 1 mol% catalyst of ^{2,7-2,7}**PyBox**⁴⁺ or 0.5 mol% catalyst of ^{2,7-2,7}**PyHC**⁸⁺ and ^{2,7-1,6}**PyHC**⁸⁺ relative to the molar charge of CEES was carried out in CD₃OD under photoirradiation at 395 nm and 450 nm. Figure 7 presents reaction-rate data—in the form of plots of conversion versus time—for the photosensitized degradation of CEES by ¹O₂, where the degradation yields exclusively CEESO, the desired sulfide product. The kinetics of the photocatalytic conversion of CEES to CEESO was followed (Supplementary Figs. 42–47) by ¹H and ¹³C NMR spectroscopy. A plausible mechanism for the formation of CEESO in preference to CEESO₂ (the much less desirable sulfone product) is presented in Supplementary Fig. 48.

The ^{2,7-2,7}**PyBox**-4Cl photocatalyst led (Fig. 7 and Supplementary Fig. 49) to full conversion of CEES to CEESO after 6 min of irradiation, yielding a conversion half-life of ~3 min. By contrast, the conversion half-life with ^{2,7-2,7}**PyHC**-8Cl as the photocatalyst is ~2 min, that is, nearly two times faster than with the cyclophane. Similar but slightly faster catalysis was observed with the compact ^{1,6-2,7}**PyHC**⁸⁺ catalysts, that is, a reaction half-life of ~1 min in both UV (395 nm) and visible (450 nm) regimes. Importantly, no detectable toxic sulfone derivative (CEESO₂) was observed for the catenane and cyclophane photocatalysts, and we detected a negligible amount of vinyl derivatives (<1%) of CEES and CEESO at the end of the reactions. All photocatalysts converted CEES to non-toxic CEESO selectively (>99%).

Previous studies have shown^{26,35} that, under the same photocatalysis conditions, unfunctionalized pyrenes led to 75% conversion of CEES to CEESO after 2h. By incorporating the pyrene photosensitizer into the pyridinium-based cyclophanes and homo[2] catenanes, we have greatly improved the rate of the reaction. The efficiency of the photocatalytic activity is attributed to many factors, such as the high solubility of these compounds resulting from the highly charged nature of the cyclophanes (4+) and catenanes (8+), the CT nature of the complex formed within the cyclophanes and catenanes enhancing the photosensitization properties of the pyrene unit, and the nanoconfinement effect of pyrene chromophores in the mechanically interlocked compounds inducing triplet quenching of the photocatalysts. Catenane 1,6-2,7PyHC8+ showed the best photocatalytic activity, which is in complete agreement with the TA and DFT studies, showing the efficient IC compared to the free cyclophane and the looser 2,7-2,7PyHC8+.

Conclusions

Three constitutionally isomeric octacationic pyrene-based homo[2] catenanes have been obtained in single one-pot self-templated syntheses on account of strong $[\pi\cdots\pi]$ interactions between the pyrenes. This efficient and tunable synthetic approach to obtain precise control of tetrachromophoric mechanically interlocked molecules can be expanded in the future to include other pyrene-based regioisomers and a variety of planar aromatic chromophores.

The TA and TD-DFT data reveal the presence of a population of triplet states following the formation of mechanical bonds. The triplet in homo[2]catenanes is characterized by a longer lifetime of

the exciplex species, which enables mixing of the spins between the partially charged separated entities and the acquisition of triplet character to the wavefunction. In addition, the nanoconfinement effect leads to efficient IC and a high level of protection, which extends the lifetime and yield of the triplet state in the pyrene-based homo[2]catenanes.

These promising photosensitization properties render this class of mechanically interlocked molecules effective as photocatalysts, as demonstrated by the model of detoxification of the sulfur-mustard simulant CEES.

Overall, this investigation highlights the benefits of using the mechanical bond to fine-tune the energy landscape of common aromatic chromophores following the development of a class of chromophores based on mechanically interlocked compounds for use as photosensitizers and photocatalysts.

Methods

NMR spectroscopic analysis. 1D and 2D NMR spectra (Supplementary Figs. 50–57) of all the pyrene-based compounds were recorded in CD₃CN.

Electrospray ionization mass spectrometry analysis. Mass spectrometry spectra (Supplementary Figs. 59–62) of all synthesized compounds were recorded. A characteristic peak of the formation of homo[2] catenanes, corresponding to [M-3] PF₆]³⁺ in the case of ^{2,7-2,7}**PyHC**·8PF₆ (Supplementary Fig. 60) and [M-3] CF₃O₂]³⁺ in the case of ^{1,6-1,6}**PyHC**·8CF₃O₂ and ^{1,6-2,7}**PyHC**·8CF₃O₂ (Supplementary Figs. 61 and 62) is present in the mass spectra and compares well with the calculated values.

X-ray crystallographic analysis. Crystallographic data for the structures are presented in Supplementary Figs. 63–65 and Supplementary Tables 1–3. The surface analysis of the crystal structure of ^{2,7-2,7}**PyHC**-8PF₆ is discussed in Supplementary Figs. 66 and 67.

Thermostability study. The thermostability of the ^{2,7-2,7}PyHC*+ was confirmed (Supplementary Fig. 68) using temperature-dependent NMR studies.

Data availability

Source data related to this paper may be requested from the authors. Crystallographic data for the structures reported in this Article have been deposited at the Cambridge Crystallographic Data Centre, under deposition numbers CCDC 2098309 (2-7-2-7PyBox-4PF₆), 2098310 (1-6-1-6PyBox-4PF₆) and 2098670 (2-7-2-7PyHC-8PF₆). Copies of the data can be obtained free of charge via https://www.ccdc.cam.ac.uk/structures.

Received: 23 September 2021; Accepted: 4 May 2022; Published online: 24 June 2022

References

- Figueira-Duarte, T. M. & Müllen, K. Pyrene-based materials for organic electronics. Chem. Rev. 111, 7260–7314 (2011).
- Mateo-Alonso, A. Pyrene-fused pyrazaacenes: from small molecules to nanoribbons. Chem. Soc. Rev. 43, 6311–6324 (2014).
- Islam, M. M., Hu, Z., Wang, Q., Redshaw, C. & Feng, X. Pyrene-based aggregation-induced emission luminogens and their applications. *Mater. Chem. Front.* 3, 762–781 (2019).
- Kinik, F. P., Ortega-Guerrero, A., Ongari, D., Ireland, C. P. & Smit, B. Pyrene-based metal-organic frameworks: from synthesis to applications. Chem. Soc. Rev. 50, 3143–3177 (2021).
- Maeda, H. et al. Alkynylpyrenes as improved pyrene-based biomolecular probes with the advantages of high fluorescence quantum yields and long absorption/emission wavelengths. Chem. Eur. J. 12, 824–831 (2006).
- 6. Zych, D. Non-K region disubstituted pyrenes (1,3-, 1,6- and 1,8-) by (hetero) aryl groups. *Molecules* **24**, 2551 (2019).
- Zych, D. & Slodek, A. Pyrene derivatives with two types of substituents at positions 1, 3, 6 and 8—fad or necessity? RSC Adv. 9, 24015–24024 (2019).
- Chang, X. et al. Coordination-driven self-assembled metallacycles incorporating pyrene: fluorescence mutability, tunability and aromatic amine sensing. J. Am. Chem. Soc. 141, 1757–1765 (2019).
- Yang, Z. et al. Hierarchical self-assembly of a pyrene-based discrete organoplatinum(II) double-metallacycle with triflate anions via hydrogen bonding and its tunable fluorescence emission. *J. Am. Chem. Soc.* 142, 13689–13694 (2020).
- Gan, K. P., Yoshio, M. & Kato, T. Columnar liquid-crystalline assemblies of X-shaped pyrene-oligothiophene conjugates: photoconductivities and mechanochromic functions. *J. Mater. Chem. C.* 4, 5073–5080 (2016).

 Feng, X., Hu, J.-Y., Redshaw, C. & Yamato, T. Functionalization of pyrene to prepare luminescent materials—typical examples of synthetic methodology. *Chem. Eur. J.* 22, 11898–11916 (2016).

- Kapf, A. et al. Alkyloxy modified pyrene fluorophores with tunable photophysical and crystalline properties. N. J. Chem. 43, 6361–6371 (2019).
- Hayer, A. et al. Highly fluorescent crystalline and liquid crystalline columnar phases of pyrene-based structures. J. Phys. Chem. B 110, 7653–7659 (2006).
- Winnik, F. M. Photophysics of preassociated pyrenes in aqueous polymer solutions and in other organized media. *Chem. Rev.* 93, 587–614 (1993).
- Pokhrel, M. R. & Bossmann, S. H. Synthesis, characterization and first application of high molecular weight polyacrylic acid derivatives possessing perfluorinated side chains and chemically linked pyrene labels. *J. Phys. Chem.* B 104, 2215–2223 (2000).
- Li, D. et al. Inorganic-organic hybrid vesicles with counterion- and pHcontrolled fluorescent properties. J. Am. Chem. Soc. 133, 14010–14016 (2011).
- Ni, X.-L., Wang, S., Zeng, X., Tao, Z. & Yamato, T. Pyrene-linked triazole-modified homooxacalix[3]arene: a unique C₃ symmetry ratiometric fluorescent chemosensor for Pb²⁺. Org. Lett. 13, 552–555 (2011).
- Ueno, A., Suzuki, I. & Osa, T. Host-guest sensory systems for detecting organic compounds by pyrene excimer fluorescence. *Anal. Chem.* 62, 2461–2466 (1990).
- Ghosh, P. et al. 'Extra stabilisation' of a pyrene based molecular couple by γ-cyclodextrin in the excited electronic state. *Phys. Chem. Chem. Phys.* 14, 11500–11507 (2012).
- Vullev, V. I., Jiang, H. & Jones, G. in Advanced Concepts in Fluorescence Sensing: Part B: Macromolecular Sensing (eds Geddes, C. D. & Lakowicz, J. R.) 211–239 (Springer, 2005).
- McNelles, S. A., Thoma, J. L., Adronov, A. & Duhamel, J. Quantitative characterization of the molecular dimensions of flexible dendritic macromolecules in solution by pyrene excimer fluorescence. *Macromolecules* 51, 1586–1590 (2018).
- Takaya, T. et al. Excited-state dynamics of pyrene incorporated into poly(substituted methylene)s: effects of dense packing of pyrenes on excimer formation. *Macromolecules* 51, 5430–5439 (2018).
- Hu, J.-Y. et al. A single-molecule excimer-emitting compound for highly efficient fluorescent organic light-emitting devices. *Chem. Commun.* 48, 8434–8436 (2012).
- 24. Jiang, W. et al. A single-molecule conformation modulating crystalline polymorph of a physical π – π pyrene dimer: blue and green emissions of a pyrene excimer. *J. Mater. Chem. C* **8**, 3367–3373 (2020).
- Miyoshi, N. & Tomita, G. Production and reaction of singlet oxygen in aqueous micellar solutions using pyrene as photosensitizer. Z. Naturforsch. B 33, 622–627 (1978).
- Liu, Y. et al. Efficient and selective oxidation of sulfur mustard using singlet oxygen generated by a pyrene-based metal-organic framework. J. Mater. Chem. A 4, 13809–13813 (2016).
- Atilgan, A., Islamoglu, T., Howarth, A. J., Hupp, J. T. & Farha, O. K. Detoxification of a sulfur mustard simulant using a BODIPY-functionalized zirconium-based metal-organic framework. ACS Appl. Mater. Interfaces 9, 24555–24560 (2017).
- Howarth, A. J. et al. Postsynthetic incorporation of a singlet oxygen photosensitizer in a metal-organic framework for fast and selective oxidative detoxification of sulfur mustard. Chem. Eur. J. 23, 214–218 (2017).
- McClure, D. S. Triplet-singlet transitions in organic molecules. Lifetime measurements of the triplet state. J. Chem. Phys. 17, 905–913 (1949).
- Kasha, M. Collisional perturbation of spin-orbital coupling and the mechanism of fluorescence quenching. A visual demonstration of the perturbation. J. Chem. Phys. 20, 71–74 (1952).
- El-Sayed, M. A. Effect of spin-orbit interactions on the dipolar nature of the radiative microwave zero-field transitions in aromatic molecules. *J. Chem. Phys.* 60, 4502–4507 (1974).
- 32. Havlas, Z. & Michl, J. Prediction of an inverse heavy-atom effect in $H-C-CH_2Br$: bromine substituent as a π acceptor. J. Am. Chem. Soc. 124, 5606–5607 (2002).
- 33. Sasikumar, D., John, A. T., Sunny, J. & Hariharan, M. Access to the triplet excited states of organic chromophores. *Chem. Soc. Rev.* 49, 6122–6140 (2020).
- Filatov, M. A. et al. BODIPY-pyrene and perylene dyads as heavy-atom-free singlet oxygen sensitizers. ChemPhotoChem 2, 606–615 (2018).
- Beldjoudi, Y. et al. Supramolecular porous organic nanocomposites for heterogeneous photocatalysis of a sulfur mustard simulant. J. Adv. Mater. 32, 2001592 (2020).
- Stoddart, J. F. Mechanically interlocked molecules (MIMs)—molecular shuttles, switches and machines (Nobel Lecture). Angew. Chem. Int. Ed. 56, 11094–11125 (2017).
- Sauvage, J.-P. From chemical topology to molecular machines (Nobel Lecture). Angew. Chem. Int. Ed. 56, 11080–11093 (2017).
- Barnes, J. C. et al. Solid-state characterization and photoinduced intramolecular electron transfer in a nanoconfined octacationic homo[2] catenane. J. Am. Chem. Soc. 136, 10569–10572 (2014).

- Inouye, M. et al. A doubly alkynylpyrene-threaded [4]rotaxane that exhibits strong circularly polarized luminescence from the spatially restricted excimer. Angew. Chem. Int. Ed. 53, 14392–14396 (2014).
- Ryan, S. T. J. et al. Energy and electron transfer dynamics within a series of perylene diimide/cyclophane systems. J. Am. Chem. Soc. 137, 15299–15307 (2015).
- 41. Hayashi, K. et al. Observation of circularly polarized luminescence of the excimer from two perylene cores in the form of [4]rotaxane. *Chem. Eur. J.* 24, 14613–14616 (2018).
- Sagara, Y. et al. Rotaxanes as mechanochromic fluorescent force transducers in polymers. J. Am. Chem. Soc. 140, 1584–1587 (2018).
- 43. Gong, X. et al. Toward a charged homo[2]catenane employing diazaperopyrenium homophilic recognition. *J. Am. Chem. Soc.* **140**, 6540–6544 (2018).
- Sagara, Y. et al. Rotaxane-based mechanophores enable polymers with mechanically switchable white photoluminescence. ACS Cent. Sci. 5, 874–881 (2019).
- David, A. H. G., Casares, R., Cuerva, J. M., Campaña, A. G. & Blanco, V. A.
 [2]rotaxane-based circularly polarized luminescence switch. *J. Am. Chem. Soc.* 141, 18064–18074 (2019).
- Özkan, M., Keser, Y., Hadi, S. E. & Tuncel, D. A. [5]rotaxane-based photosensitizer for photodynamic therapy. *Eur. J. Org. Chem.* 21, 3534–3541 (2019).
- Garci, A. et al. Mechanical-bond-induced exciplex fluorescence in an anthracene-based homo[2]catenane. J. Am. Chem. Soc. 142, 7956–7967 (2020).
- 48. Li, W.-J. et al. Rotaxane-branched dendrimers with enhanced photosensitization. J. Am. Chem. Soc. 142, 16748–16756 (2020).
- Li, W.-J. et al. AIE-active chiral [3] rotaxanes with switchable circularly polarized luminescence. Angew. Chem. Int. Ed. 60, 9507–9515 (2021).
- Rajamalli, P. et al. Using the mechanical bond to tune the performance of a thermally activated delayed fluorescence emitter. *Angew. Chem. Int. Ed.* 60, 12066–12073 (2021).
- Stoddart, J. F. The chemistry of the mechanical bond. Chem. Soc. Rev. 38, 1802–1820 (2009).
- Barin, G., Coskun, A., Fouda, M. M. G. & Stoddart, J. F. Mechanically interlocked molecules assembled by π–π recognition. *ChemPlusChem* 77, 159–185 (2012).
- Lewis, J. E. M., Galli, M. & Goldup, S. M. Properties and emerging applications of mechanically interlocked ligands. *Chem. Commun.* 53, 298–312 (2017).
- Barnes, J. C. et al. A radically configurable six-state compound. Science 339, 429–433 (2013).
- Jiao, Y. et al. A donor-acceptor [2] catenane for visible light photocatalysis. J. Am. Chem. Soc. 143, 8000–8010 (2021).
- Barnes, J. C. et al. ExBox: a polycyclic aromatic hydrocarbon scavenger. J. Am. Chem. Soc. 135, 183–192 (2013).
- Juríček, M. et al. Ex²Box: interdependent modes of binding in a two-nanometer-long synthetic receptor. J. Am. Chem. Soc. 135, 12736–12746 (2013).
- 58. Juríček, M. et al. An Exbox[2]catenane. Chem. Sci. 5, 2724–2731 (2014).

- Lu, Q. et al. Comparison study of the site-effect on regioisomeric pyridyl-pyrene conjugates: synthesis, structures and photophysical properties. J. Org. Chem. 85, 4256–4266 (2020).
- Austin, A. et al. A density functional with spherical atom dispersion terms.
 J. Chem. Theory Comput. 8, 4989–5007 (2012).

Acknowledgements

We thank Northwestern University (NU) for their continued support of this research. This research was also supported by the National Science Foundation under grant no. DMR-2003739 (M.R.W. and R.M.Y., photophysical studies). O.K.E. acknowledges support from the Defense Threat Reduction Agency under award no. HDTRA1-19-1-0010. L.O.J and G.C.S were supported by the Department of Energy, Office of Basic Energy Science as part of the Center for Bioinspired Energy Science under grant DE-SC0000989. We thank C. Lin for his assistance with fluorescence quantum yield measurements and S. Abid and A. H. G. David for helpful discussions. The research made use of the Integrated Molecular Structure and Educational Research Center (IMSERC) at NU, which receives support from the State of Illinois and the International Institute for Nanotechnology (IIN). The research was also supported in part through the computational resources and staff contributions provided for the Quest High Performance Computing Facility at Northwestern University, which is jointly supported by the Office of the Provost, the Office for Research, and Northwestern University Information Technology.

Author contributions

A.G. and J.F.S. conceived the project. A.G. carried out the synthesis. J.A.W. and L.O.J. conducted the computational study. A.G. and R.M.Y. performed the optical study. A.G., Y.B. and A.A. carried out the photocatalytic experiments. M.O. contributed to the graphical design in the figures. A.G. and W.L. studied the dynamic behaviour of the catenane. C.L.S. resolved the crystal structures. M.K.-R. contributed to the HPLC, electrospray ionization mass spectrometry and NMR titrations. A.G., J.A.W., R.M.Y. and J.F.S. wrote the draft manuscript. All other co-authors contributed to various stages of manuscript preparation.

Competing interests

A.G. and J.F.S. have filed a patent application lodged with Northwestern University based on this work (Invention Disclosure: Disc-ID-22-04-22-002). The other authors declare no competing interests.

Additional information

 $\label{thm:continuous} \textbf{Supplementary information} \ The online version contains supplementary material available at $$https://doi.org/10.1038/s41929-022-00799-y.$$

Correspondence and requests for materials should be addressed to J. Fraser Stoddart.

Peer review information Nature Catalysis thanks Diego Troya and the other, anonymous, reviewer(s) for their contribution to the peer review of this work.

Reprints and permissions information is available at www.nature.com/reprints.

Publisher's note Springer Nature remains neutral with regard to jurisdictional claims in published maps and institutional affiliations.

 $\ensuremath{\texttt{@}}$ The Author(s), under exclusive licence to Springer Nature Limited 2022